International Journal of Multidisciplinary Research and Growth Evaluation.

Uncovering soil piping vulnerability using direct current geophysical techniques in Awka, Anambra State, Nigeria

Chibuogwu IU [1*], **Ugwu GZ** [2]
[1] Nnamdi Azikiwe University Awka, Anambra, Nigeria
[2] Enugu State University of Science and Technology Agbani, Enugu, Nigeria

* Corresponding Author: **Chibuogwu IU**

Article Info

ISSN (online): 2582-7138
Volume: 04
Issue: 03
May-June 2023
Received: 17-04-2023;
Accepted: 02-05-2023
Page No: 426-440

Abstract
In recent times, there have been increasing reports of soil subsidence occurring in various parts of Anambra State, Nigeria. The formation of soil pipes in the subsurface, which has been reported by many researchers globally, is the chief cause of these subsidence incidents. Thus, this research aims to use Direct Current (DC) geophysical techniques to delineate the spatial distribution, pattern, and characteristics of these soil pipes at two sites: Awka Site 1 and Awka Site 2 both in Awka South LGA of Anambra state, Nigeria. Two electrodes array configurations - the dipole-dipole array for analyzing the Electrical Resistivity Tomography (ERT) and the Schlumberger array for analyzing the Vertical Electrical Sounding (VES) - were employed. Nine ERT profiles and eighteen soundings were carried out. The results from the ERT survey divided the subsurface into six distinct structures. The high-resistivity 3000-30000Ωm, the eroded structure with dry pore spaces, which mainly occur at the top of the profile, was interpreted as having the right conditions for the formation of soil pipes. The result from the VES survey revealed two to five different geo-electrical sections and fourteen distinctive sounding curves that are characterized by the vertical changes in the subsurface. The weathered soil with resistivity ranging from 1200-30000Ωm, which aggregates very close to the surface 0-5m of the study areas, was interpreted as having the best soil formations that allow the building of soil pipes. The 2D and 3D iso-resistivity maps obtained from the data of the VES show that soil pipes follow the NW-SE direction. This coincides with the stress direction, fluid migration paths, and sloppy terrains of the study areas.

DOI: https://doi.org/10.54660/.IJMRGE.2023.4.3.426-450

Keywords: Soil piping; Tunnel erosion; Erosion; Soil Subsidence; VES; Dipole-Dipole; Resistivity; Conductivity; Dispersion

Introduction

Soil grains are small particles that aggregate to form a soil mass, but they remain uncompacted and contain empty spaces known as voids that allow fluids to pass through via a process called seepage (Dodds, 2003). Exogenic processes, such as weathering, cause soil grains to continually move from one location to another, resulting in a state of motion called erosion (Onda, 1994) [29]. Erosion is not only a geomorphological process but also a form of land degradation that can be caused by both overland and subsurface flow of fluids. Overland flow typically triggers sheet, rill, or gully erosion and is extensively researched and documented. Conversely, subsurface flow leads to tunnel erosion or soil piping, which is a silent yet equally hazardous form of erosion that lacks appropriate recognition, akin to overland flow processes (Bernatek-Jakiel & Poesen, 2018) [3].

The soil piping here may be defined as the hydraulic removal of soil in the subsurface by fluid flow, which usually leads to the formation of underground channels called pipes (Bernatek-Jakiel & Kondracka, 2016; García-Ruiz *et al*., 1997; Wilson *et al*., 2018) [2, 13, 38].

It usually begins as small pores called flute holes within the subsurface and with time (Bryan, 2000; Holden & Burt, 2002) [8, 19], it can grow large enough to form conduits leading to different channels more permeable than the surrounding materials, where water, soil grains and air can pass through (Parker *et al*., 1990) [31]. As the flow rates increase through these channels, they further corrode the conduit that was created, leading to the erosion of the subsoil and collapsing of the structure above the subsurface (Bernatek-Jakiel & Wrońska-Wałach, 2018; Graham & Lin, 2012; Jones *et al*., 1997) [3, 17, 21, 4]. These will eventually create a surface gully or sinkhole called Land Subsidence (Graham & Lin, 2012; Parker *et al*., 1990; Sidle *et al*., 1995) [17, 31, 34].

The settling or sinking of the Earth's surface due to the removal of its materials is known as land subsidence (Verachtert *et al*., 2011; Zhang & Wilson, 2013; Zhu *et al*., 2002) [37, 39, 40]. This phenomenon presents a significant environmental problem for both developed and developing communities, as it can cause changes in elevation and damage to structures (Zhang & Wilson, 2013) [39]. Furthermore, land subsidence can exacerbate flooding and decrease the capacity of aquifers to store water (Atallah *et al*., 2015) [1]. This issue is particularly troublesome in regions that experience frequent precipitation and flooding, as well as areas where water and air moisture can permeate the soil at a high rate (Atallah *et al*., 2015; Bernatek-Jakiel & Wrońska-Wałach, 2018; Patti *et al*., 2021) [1, 4, 32]. Given these factors, it is no surprise that the study area exhibits characteristics that make it susceptible to land subsidence (Chibuogwu & Ugwu, 2023) [12].

In addition to the above, land subsidence can occur in different climatic region from the temperate zone through the arid and semi-arid zones to the tropical zone. It can also occur at different vegetation and geological settings making it a global environmental issue (Bernatek-Jakiel & Poesen, 2018; Castañeda *et al*., 2017; Jones *et al*., 1997; Mi *et al*., 2013; Parker *et al*., 1990; Vannoppen *et al*., 2017) [4, 31, 21].

Land subsidence is a complex problem without a clear-cut solution(Blanco-Canqui and Lal, 2010; Wilson *et al*., 2018) [38], primarily due to the intricate hydrological networks created by soil-piping paths, which remain hidden beneath the soil surface (Bernatek-Jakiel and Kondracka, 2016; Holden, 2004) [2, 18]. As a result of this, studying the characteristics of land subsidence can be challenging to quantify (Patti *et al*., 2021) [32]. However, there are efficient and non-invasive methods of investigation that can be employed to determine the extent of subsidence buildup without carrying out a major excavation procedure that would necessitate heavy machinery and disrupt the topsoil(Bernatek-Jakiel & Kondracka, 2016) [2]. By utilizing geophysical techniques, we can directly investigate the depth and location of soil-piping paths, providing a clearer picture of the issue (Carrazza *et al*., 2016; Holden, 2004; Mi *et al*., 2013; Ungureanu *et al*., 2017) [10, 18].

In order to effectively detect tunnel erosion using geophysical techniques, researchers must be familiar with the intricacies of conducting a geophysical survey and the specific instruments necessary for resolving the geological complexity of soil pipe formation in the overburden. Additionally, understanding the water circulation pattern is crucial in accurately interpreting the geophysical evidence as geological features. Failure to do so may result in ambiguous or misleading data. By ensuring a comprehensive and nuanced understanding of the geophysical survey, researchers can effectively detect tunnel erosion and provide accurate data on subsurface soil conditions.

In this study, we aimed to investigate the spatial distribution, pattern, and characteristics of soil pipes in an area of known soil subsidence in Awka, Anambra State, Nigeria. To achieve this goal, we employed two direct current techniques: Electrical Resistivity Tomography (ERT) and Vertical Electrical Sounding (VES). These methods were used to gain a better understanding of the complexity and characteristics of the soil-piping network. By utilizing ERT and VES, we were able to achieve a more comprehensive understanding of the subsurface soil conditions in the area.

Geology and lithostratigraphic of study area

The study area is part of the Anambra Sedimentary Basin in southeastern Nigeria (figure 1). The Anambra Basin covers about 40,000 km2 (ESMP, 2016; Chibuogwu and Ugwu, 2003,) [12].

The southern boundary coincides with the delta swamps of the Niger Delta Basin and extends northward beyond the Bende Ameki Formation. The basin is believed to have formed in conjunction with the folding and uplift of the Abakaliki-Benue area during the Santonian era. The Anambra Basin is the major center of depocentre of clastic deposits and deltaic sequences resulting from the second Lower Benue Trough tectonic activity figure 1a shows the geological map of Nigeria and Anambra basin.

The soils of Anambra State particularly have groundwater reservoirs that severely contribute to ecological problems in the region. They are mainly typified by the coastal plain sands and are highly susceptible to erosion. Beneath the weak lateritic and acidic soils are unstable and poorly consolidated geologic rocks and material. The sandy members of these geologic units contain huge groundwater reservoirs that are referred to as aquifers with pore water pressures that become threatening when overlying structures carry uncompromising loads. The lateritic and sandy soils are easily eroded by storm water runoffs, (ESMP, 2016; Chibuogwu and Ugwu, 2023) [12].

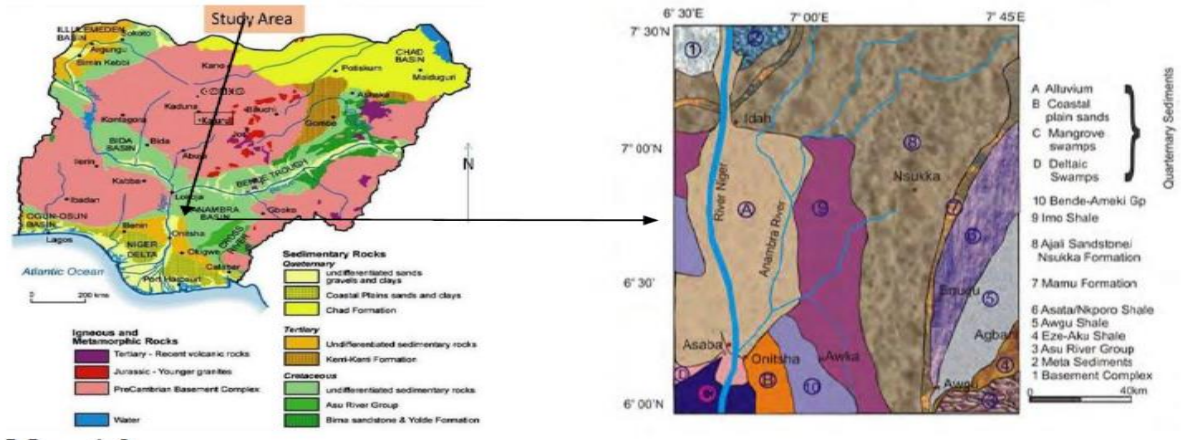

Fig 1: Map of the geological setting of Nigeria and Anambra Basin

Study Area

This study focuses on two sites in Awka (figure 2), the capital of Anambra State, Nigeria, located at (Lat. 6.2220E and Long 7.0821E). Awka Site 1 is located in close proximity to Paul University, Awka, with a geographical coordinate of (6.22320N and 7.08240E). The piping hole at this site, measuring approximately 5cm in diameter, has caused significant damage to the constructed road; resulting in double sinkholes (soil subsidence) with a diameter of approximately 70cm (see Figure 3). Awka Site 2 is located at the Jerome Udorji Secretariat with a geographical coordinate of (6.22200N and 7.08190E). The piping hole at this site has been present for approximately three years; creating multiple holes with an average diameter of 10cm, as well as a visible sinkhole approximately, 300cm in diameter (see Figure 4). By examining these two sites in detail, we can gain greater insight into the characteristics and formation of soil pipes in areas of subsidence.

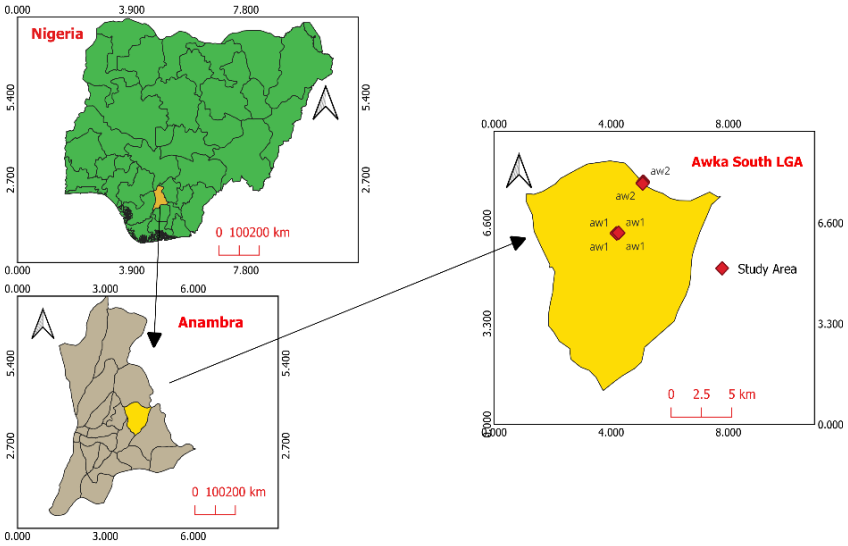

Fig 2: Map showing the surveyed state and LGA

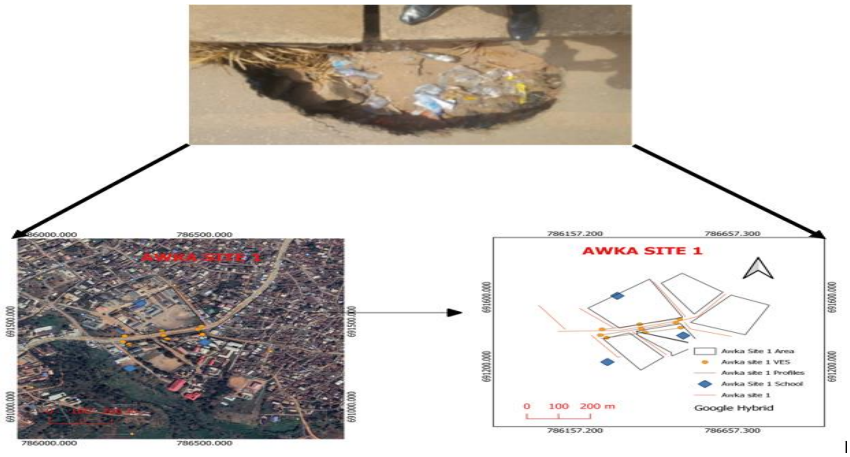

Fig 3: Map of Awka site 1 showing the subsidence, satellite image and survey points

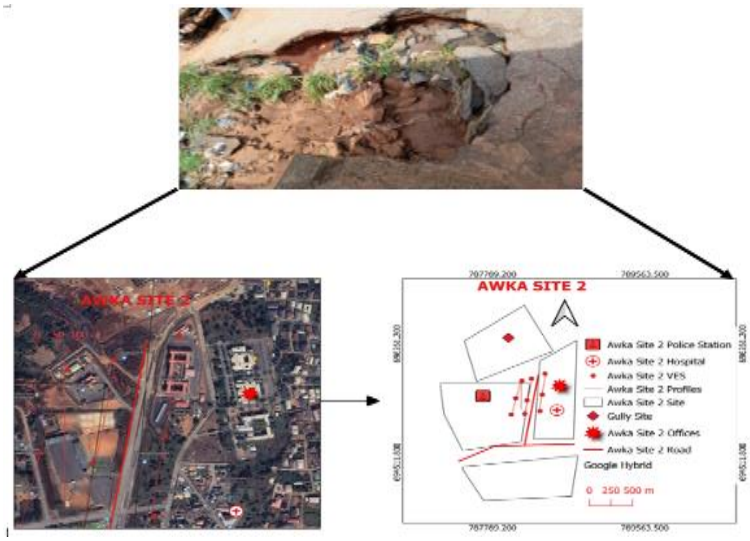

Fig 4: Map of Awka site 2 showing the subsidence, satellite image and survey point

Method

The DC method utilized in geophysics involves creating an electric field via injection of an electric current (I) through metal rods known as the transmitter circuit (Carrazza *et al*., 2016) [10]. As a result of this field, electrical potential (ΔV) is generated, which can then be intercepted by metal or non-polarized electrodes, collectively known as the receiver circuit. By using these methods, researchers can accurately examine the electrical properties of materials and the underlying geology of subsurface environments (Loke & Barker, 1996) [26].

Data acquisition is made possible by the iteration of the material with known properties in order to measure the electrical potential after generating and injecting current into the soil. The lateral variation shows information about heterogenties that is related to mineral constitution or geological structures such as fault, dikes contact etc (Carrazza *et al*., 2016) [10].

Electrical Resistivity Tomography (ERT) is commonly used to identify natural cavities, or "soil pipes," by exploiting the differences in electrical properties between mineral grains and the absence of these properties in the cavities. Furthermore, soil pipes are typically hollow tunnels that can be filled with air, water, or collapsed soil materials, meaning that they have a different resistivity from the surrounding structure that can be easily detected through electrical resistivity surveys. Factors such as the depth of the cavities, soil thickness, changes in the phreatic level, and weather conditions (such as dry or rainy seasons) can all impact how the soil pipe is filled, further affecting its resistivity signature. With the ability to detect these subtle differences, ERT is a powerful tool for identifying and characterizing soil pipes in subsurface environments (Cardarelli *et al*., 2014; Leslie and Heinse, 2013; Mi *et al*., 2013; Patti *et al*., 2021) [9, 23, 32].

Dipole-Dipole Method

The measurement of soil pipes and their spatial distribution for this study utilized the dipole-dipole electrode configuration due to its superior horizontal resolution and greater coverage depth in subsurface spaces (Neyamadpour *et al*., 2010) [28]. This particular configuration consists of two pairs of electrodes: a current electrode (transmitter) and a potential electrode (receiver). A dipole is formed by setting two electrodes closely together at one end, and convention dictates that the distance between the current and potential electrodes is maintained at an equal distance (spacing = a) with each distance being an integer multiple of "a" (J. O. Coker *et al*., 2020; Li and Rao, 2019) [20, 25]. By utilizing this setup, the researchers were able to accurately measure the nature and spatial distribution of soil pipes with high precision and accuracy.

The resistivity survey for this study used a PASI resistivimeter with 24 steel electrodes spaced at 5 meters to achieve a profile length of 100 meters or more, depending on available space. To minimize errors in the survey, all electrodes underwent a constant resistance test at regular intervals prior to the survey, with a maximum desired limit for ground resistance (Rg) set at 10KΩ. Any electrodes with an Rg value above this limit were deemed to have poor contact with the ground and subsequently adjusted by measures such as hammering or applying saline solution, after which the PASI resistivimeter was activated for the actual survey.

The PASI resistivimeter was utilized for the purpose of measuring and collecting resistivity data. The gathered information was then analyzed using DEPROWIN software, which allowed for the development of 2D electrical imaging pseudosections constructed from the measured physical parameters. The program was specifically designed to facilitate inversion of extensive data ranging from 200 to 21000, by utilizing a system consisting of numerous electrodes spanning from 20 to 16000. The pseudosections are divided into rectangular blocks, which are then represented through the optimization of field measurements. This optimization technique works to minimize the difference between the calculated and measured apparent resistivity values by adjusting the model resistivity of the block. This difference is then expressed as the RMS (Root Mean Square) error, as outlined by (Carrazza *et al*., 2016; Loke & Barker, 1996) [10, 26].

Vertical Electrical Sounding Method

The Vertical Electrical Sounding (VES) for this study was carried out using the Schlumberger electrical array (Olafisoye, 2013; Zohdy *et al*., 1974) [42] and the Pasi resistivity meter was used to measure the apparent resistivity. Eighteen electrical soundings were completed (Figs 3 and 4) with a maximum half current electrode spacing (AB/2) of

100m. The field data were then analysed using the partial curve matching technique (Gouet *et al*., 2020; Koefoed, 1979; Olafisoye, 2013) [43], using master curves (Olafisoye, 2013; Orellana and Mooney, 1966) and sets of auxiliary diagrams (Olafisoye, 2013; Zohdy, 1965; Keller and Frischnecht, 1966) [41] to provide initial estimates of the resistivity and thickness of the various geoelectric layers for each VES location. These geoelectric parameters were used as initial models for computerised iteration using IpI2win software (Vander Velpen, 1988). Partial curve fitting analysis resulted in a 3-5 layer (resistive-conductive-resistive) curve model for the eighteen VES surveyed.

Results

Result for Dipole-Dipole

In this comparative study, the 2D resistivity imaging data collected via the dipole-dipole array were subjected to a robust inversion method. The inversion process involved nine iterations, at the completion, the process had converged with an RMS misfit of 7.39%. Six distinct images were then generated through the process, which are outlined in Profile 1 through Profile 6.

Figure 5 and Figure 6 provide an overview of the inversion process carried out on Profiles 1 through 3 at Awka site 1 and on Profiles 4 through 6 at Awka site 2. The orientation of each profile was chosen to match the NW-SE direction of the study area, taking into consideration the strain directions of the subsurface materials and to reduce the anisotropic effect. The first observation made from the inversion output shows that the profiles exhibit anisotropic resistivity distribution, leading to six distinct structures labeled A, B, C, D, P, and bedrock. Structure A, represented by blue colors, refers to the fault or fracture zone with saturated content. Structure B, identified with green color, corresponds to clay. Sandy clay is represented by the yellow-colored structure C, while structure D, identified by the red color, corresponds to sand. The letter P is used to identify an eroded structure illustrated by purple color, which could potentially be the location for soil pipes. Finally, the bedrock is used to represent the lowest layer.

Profile 1

This profile was placed 3 meters west of a known soil pipe (Figure 5a) and surveyed over a length of 200 meters using an electrode spacing of 5 meters. The maximum depth probed was 25 meters, with resistivity values ranging from 1 to 400 Ωm. The top of the profile reveals a finely stretched structure labelled D with resistivity ~250 Ωm. Within this structure are the zones with the highest resistivity ~ 400Ωm, labeled P. they come in three different patches. The first patch is located at the northern end of the profile within electrodes 20 -30 at a depth of 3m while the other patches are located at the center of the profile beneath electrodes 65 and 95 respectively and at a depth of 5m. The low- resistivity zones, labelled A, with an approximate resistivity of 20Ωm are well imaged. They may be considered to be saturated with water. Sandwiching the water-bearing zone is the clay labelled C with resistivity ~180Ωm.

Profile 2

Profile 2 was laid directly on top of the soil pipe (figure 5b). A profile length of 100m was surveyed with an electrode spacing of 5m and a maximum depth of 25m was probed. The profile is characterized by resistivity ranging from 899 - 38999Ωm. The inversion output described similar anisotropic structures like those in profile 1. At the top of the profile is the zone labeled D, the fine sand with an approximate resistivity of 16000 Ωm. Within this zone (D) are patches labeled P, the eroded soils, with very high resistivity ~38999 Ωm, located at the northern and at the center of the profile. At the extreme south of the profile is a squared zone known as the bedrock with resistive that is way beyond 40000 Ωm. Surrounding these high resistivity zones are regions with bright yellow colour, labeled C with resistivity of ~7500 Ωm and just below the region are the clayey soil, labeled B with an approximate resistivity of 3161 Ωm. The zone label A, with resistivity of ~ 900 Ωm is saturated with water.

Profile 3

Profile 3, (figure 5c) was laid 3m east of the soil pipe. A profile length of 100m was surveyed with an electrode spacing of 5m. As in the two previous profiles, a maximum depth of 25m was probed. The profile is characterized by resistivity ranging from 39 - 1199 Ωm. At the top of the profile is a zone considered to be composed of saturated materials penetrating a depth of 5m with a very low resistivity of ~40 Ωm. They can be observed in four patches, scattered at different part of the profile. Surrounding the saturated materials is the clay zone labeled B with resistivity of ~100 Ωm. The thick purple region that covers about 70% of the profile is interpreted as bedrock. In between the bedrock and the clayey zone are two thin region- labelled C and D – highly stratified with intermediate resistivity, approximately 200 Ωm and 400 Ωm respectively, cutting from one end of the profile to the other.

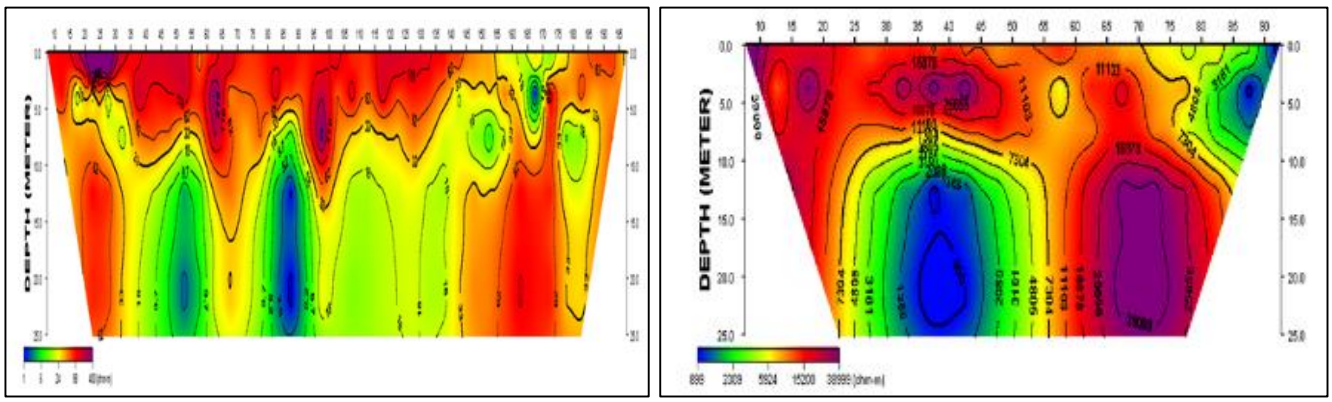

(a) (b)

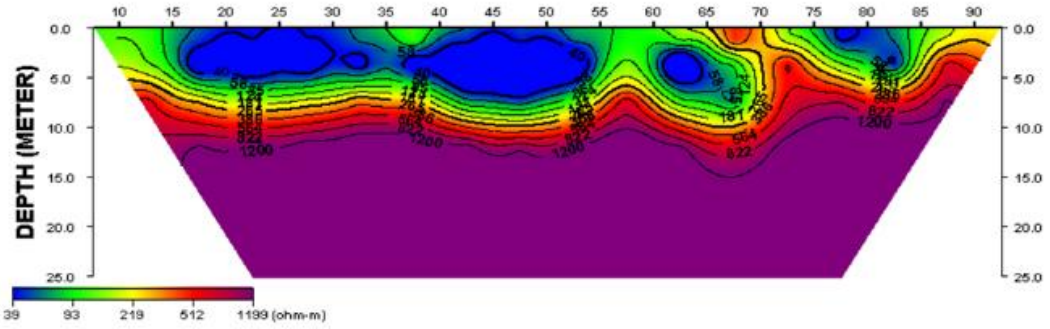

(c)

Fig 5: Pseudo-section of the dipole-dipole array for Awka site 1

Profile 4

Profile 4 was laid 3m west of the soil subsidence figure 6a. A profile length of 100m was surveyed with an electrode spacing of 5m. The depth probed was 25m. The resistivity for this profile ranges from 149 – 110000 Ωm. At the top of the profile, between electrode 25 and 30 is the zone labeled P with an approximate resistivity of 80000 Ωm that is penetrating a depth of 3m. The zone is considered to be filled with eroded structures. Sandwiching this high resistivity is a thin structure, labelled B, the clayey zone with resistivity of ~1000 Ωm. This zone acts like a blanket that prevents further erosion to occur in the profile. Covering 60% of the profile is the bedrock with a very high resistivity that is more than 110000 Ωm.

Profile 5

Profile 5 was laid on the top of the soil subsidence figure 6b. The profile length surveyed is 100m and a depth of 25m was probed with an electrode spacing of 5m. The range of resistivity for this profile is characterized from 149 - 330000 Ωm. The top of the profile shows region with topsoil materials having a low resistivity of ~200 Ωm and reaching a depth of 2m, these regions coincide with the soil subsidence at the top of the profile. A thin layer of clay soil, labeled B with resistivity of ~1000 Ωm, stretches beneath the topsoil from one end of the profile to the other end, preventing the penetration of topsoil materials and the formation of soil pipes in the subsurface. There are also stratified zones labeled C and D, which are sandy clay and fine sands, and are stretching thinly across the profile, just beneath the clayey soil.

Profile 6

Profile 6 was placed 3 meters east of the soil subsidence figure 6c and surveyed to a length of 100 meters with a probe depth of 25 meters and electrode spacing of 5 meters. The measured resistivity of this profile varied from 49 to 499,999 Ωm across the surveyed area. Just like in Profile 4, the top of Profile 6 revealed patches of thick, clayey soil labeled as 'B', which had an approximate resistivity of 400Ωm that prevents topsoil material penetration and tunnel erosion formation. On the surface of the profile, a zone of fine sand labeled as 'D' with an approximate resistivity of 20,000Ωm was detected between the electrode spacing of 25 and 30 meters, which coincides with the labeled 'P' portion of Profile 4. It can indicate that soil piping forms in these regions.

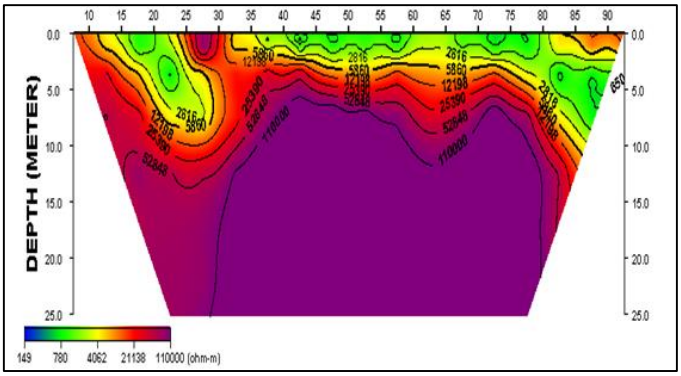

(a)

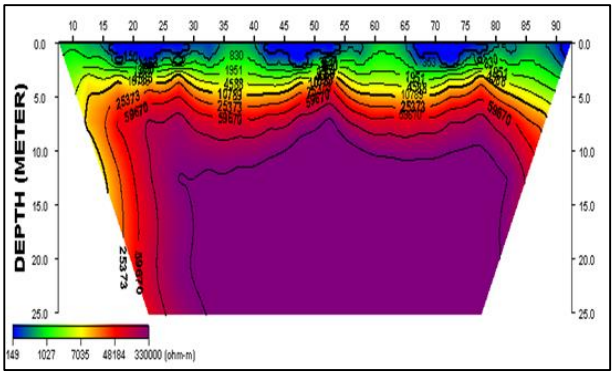

(b)

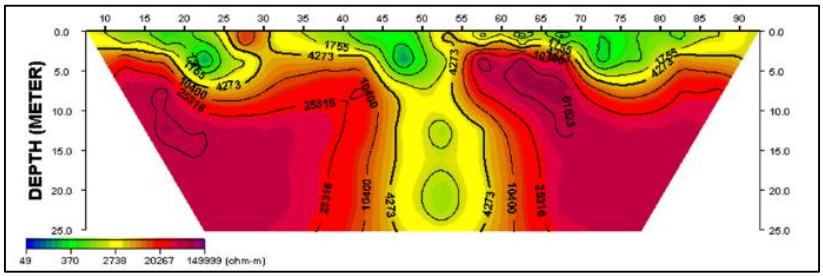

(c)

Fig 6: Pseudo-section of the dipole-dipole array for Awka site 2

Result for Vertical Electrical Sounding

Figures 7 and 8 present the VES curves obtained from the survey by plotting the observed apparent resistivity gotten from the field against the half-electrode spacing (AB/2) or depth below the subsurface on a bi-logarithmic graph. The curves were interpreted manually by partially matching the different master curves. After which, they were digitally generated using the IPI2win computer software and ensuring the lowest RMS-error for each model. The solid line overlaid on the observed curve represents the theoretical curve for the best-fit model for the sounding. The blue blocks on the graph indicate the distribution of the true resistivity value (ρ), depth (e), and thickness (t) of the geological layers.

The occurrence of the curves is in such a way that they characterize the horizontal and vertical variety of the layers in the study profiles. Table 1 and 2, show the distribution layers with different soundings. The curves types that correlates with the distributed layers are identified as H, K, KA, HA, HK, AK, HKQ, HKH, KHK, AKQ, and KHA for both study areas. They describe two to five geo-electric layers due to the vertical electrical anisotropic properties of the study areas. The AK curve in Awka site 1 dominates with 33.3% frequency, while the HK, HKH and KHK occur more than once for both sites with a 22.2% frequency. The rest of the curves occur just once with a percentage 11.1%.

The curves from the bi-logarithm graph (figure 7 and 8) were used to generate the geo-electric sections. The geo-electric sections show the vertical changes of layers along each profile in the subsurface until about a depth of 84m and 35m for Awka site I and Awka site II respectively. The vertical changes, in addition to the electrical characteristic of the subsurface (resistivity ρ, thickness t, and depth e), delineated three to five distinctive geo-electric layers. The most occurred layer, predominately in Awka site I (figure 11) is the weathered decayed soil with resistivity of $1200 < \rho < 30000\Omega m$. Soil pipes or tunnels may form in the layer within depth of $0 < e < 6m$. These may be because the high resistivity at this depth encourages dispersion in the soil that increases seepage pressure. (Bhagyalekshmi *et al*., 2015; Joshi *et al*., 2021; Onda, 1994) [5, 22, 29].

At the other end of the geo-electric section is a thin layered structure, the conductive soil with very low resistivity $10 < \rho < 100\Omega m$, predominate in Awka site 2 (figure 12). They may be considered as contaminated topsoil as they occur close to the surface of the profile $0 < e < 2m$. They act as a blanket to prevent excessive seepage flow, which discourages the formation of soil pipes. Other geo-electric layers include topsoil ($100 < \rho < 1000\Omega m$), lateritic soil ($500 < \rho < 3000\Omega m$), fractured soil ($3000 < \rho < 90000\Omega m$) and Basement ($40\Omega m < \rho < \infty$).

Iso-resistivity Map

The extents of the paths created by soil pipes were estimated by mapping out the true resistivity generated from the values of the different geo-electric layers and GPS coordinates from the sites (figure 9 and 10). From the forgoing evidences of the results obtained in the dipole-dipole survey, the lithological models and literatures (Borah *et al*., 2022; Gibson *et al*., 2004; Got *et al*., 2020; Joshi *et al*., 2021; S. Li *et al*., 2015; Mi *et al*., 2013) [7, 14, 16, 22], it is inferred that soil pipes form very close to the surface. Thus, the depth considered for the mapping ranges from 0 – 5m. The anti-synclinal nature at the center of the maps (point of highest resistivity), VES 5 and VES 2 for Awka site I, and VES 3 for Awka Site II, show the inlet and outlet points of the soil pipe. A critical view of the map also helps decipher the possible migration paths of the soil pipes as NE – SW for Awka site I and for Awka site 2, which is similar to the stress direction (Ogbe and Osokor, 2020 and Amugu *et al*., 2010) and the travel path of rainwater in the study areas. Thus, it may be assumed that soil pipes depend on water flow paths. Which travel from higher altitudes to low altitudes (gravity dependent). Hence, they form easily at sloppy terrains (Bhagyalekshmi *et al*., 2015; Gilman & Newson, 1980; Onda, 1994; Pierson, 1983) [5, 29, 33].

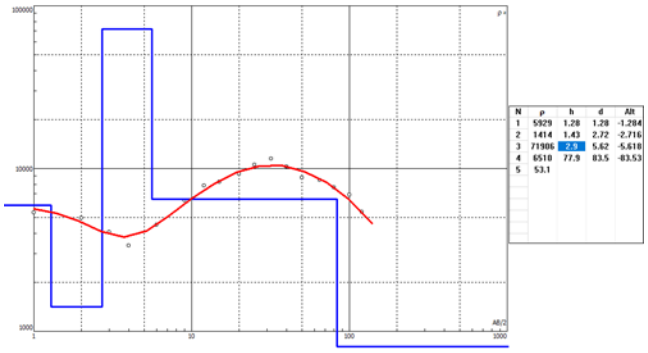

(a)

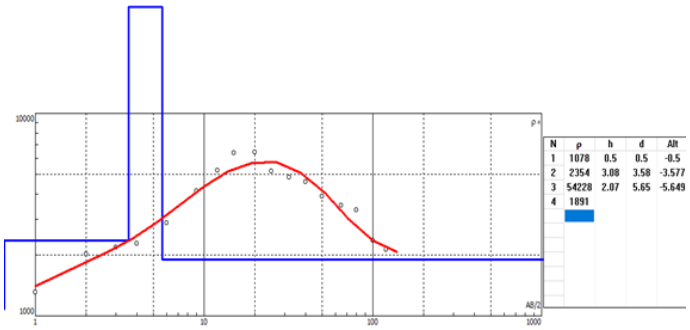

(b)

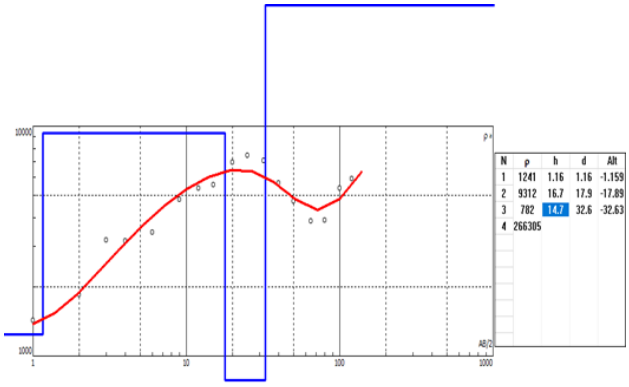

(c)

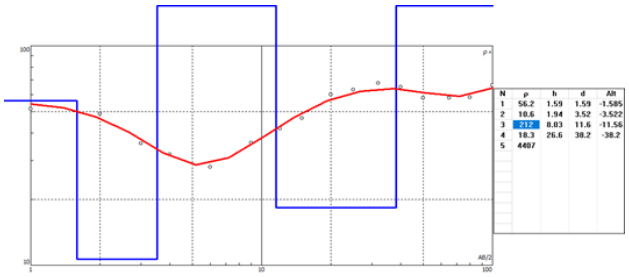

(d)

Fig 7: Four representation of the nine Vertical Electrical Sounding curves for Awka site 1

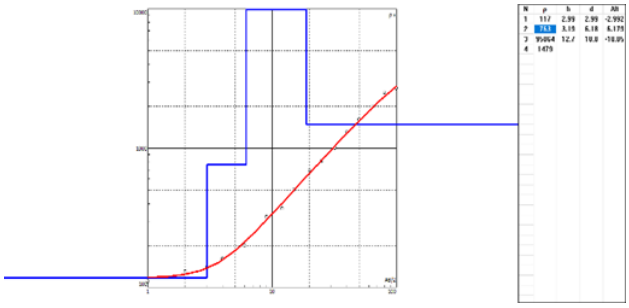

(a)

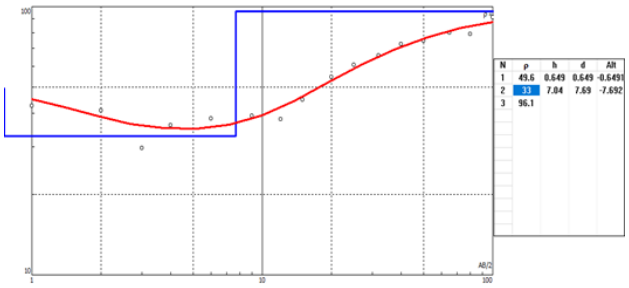

(b)

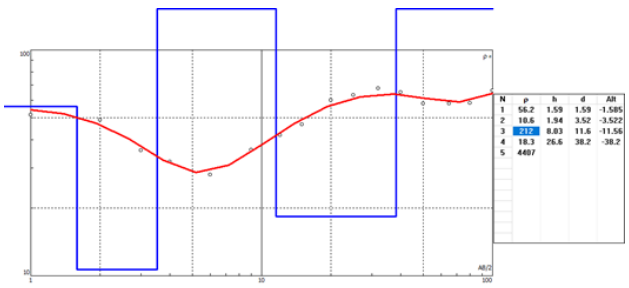

(c)

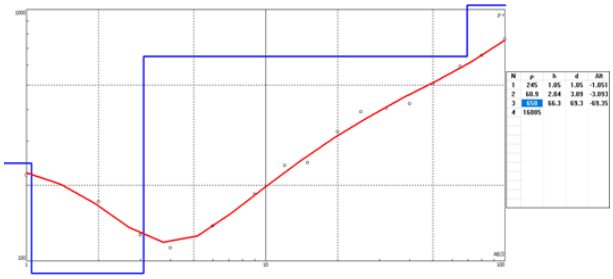

(d)

Fig 8: Four representation of the nine Vertical Electrical Sounding curves for Awka site 2

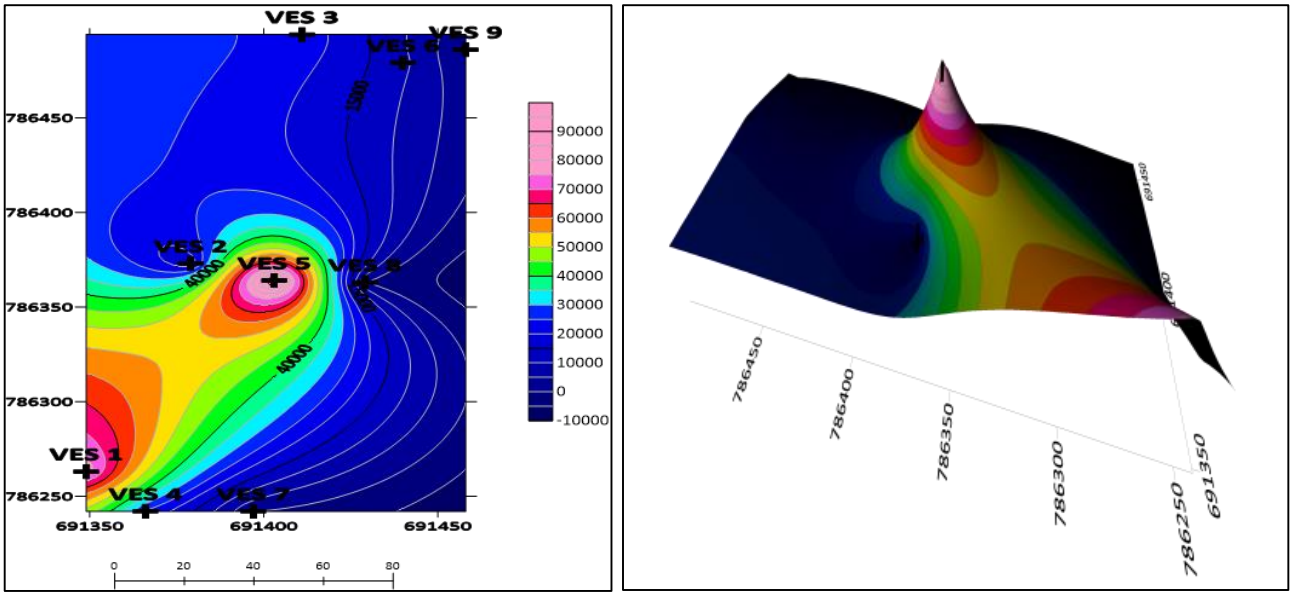

Fig 9: 2D and 3D Iso-resistivity graph for Awka site 1

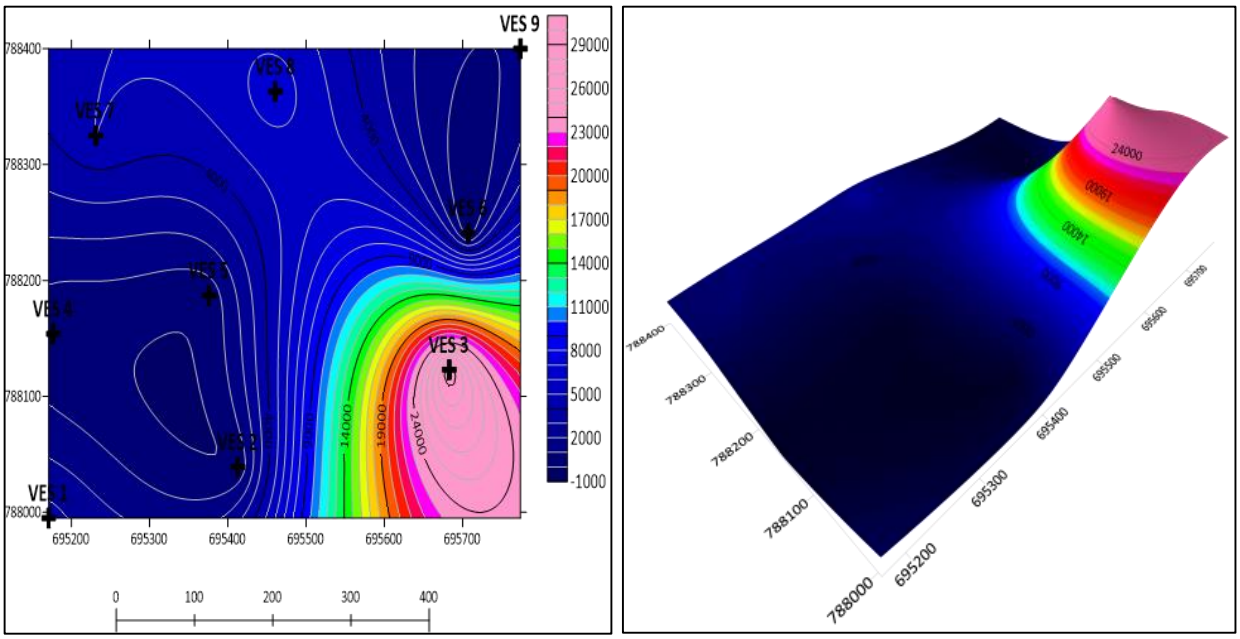

Fig 10: 2D and 3D Iso-resistivity graph for Awka site 2

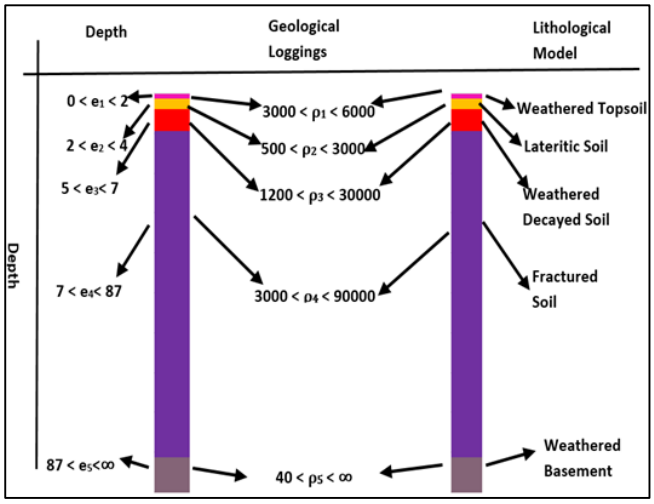

(a)

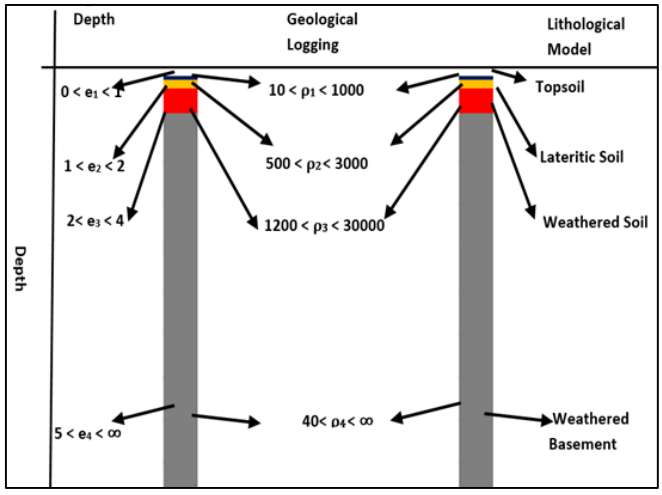

(b)

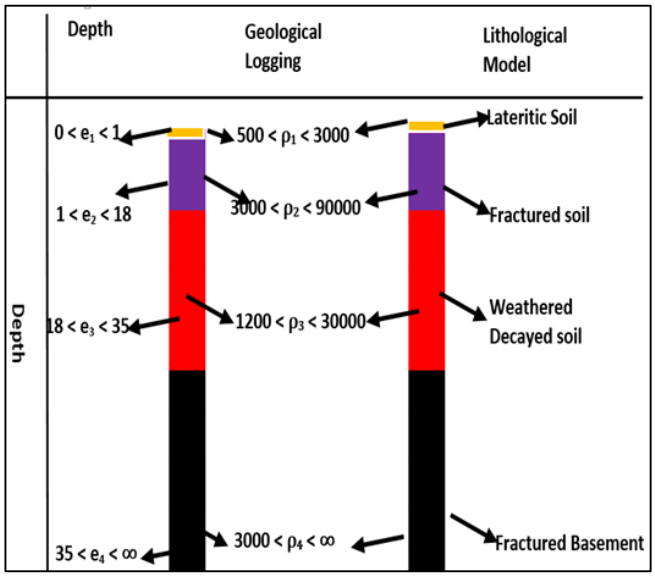

(c)

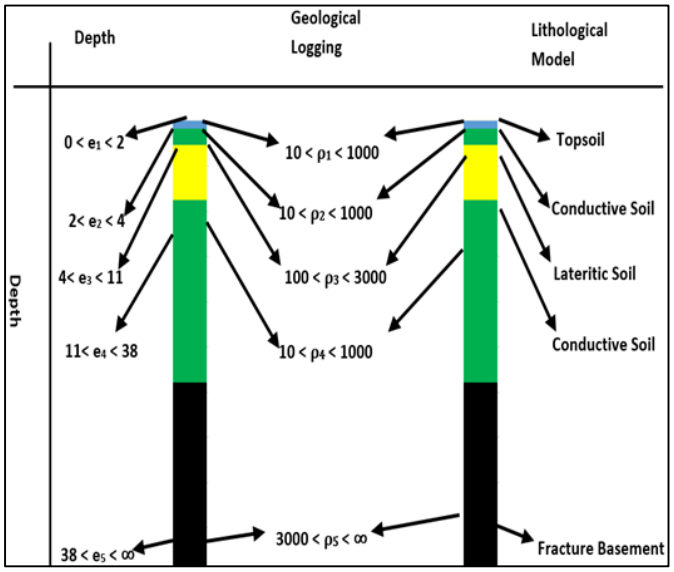

(d)

Fig 11: Four representation of the nine Geo-electric section for Awka site 1

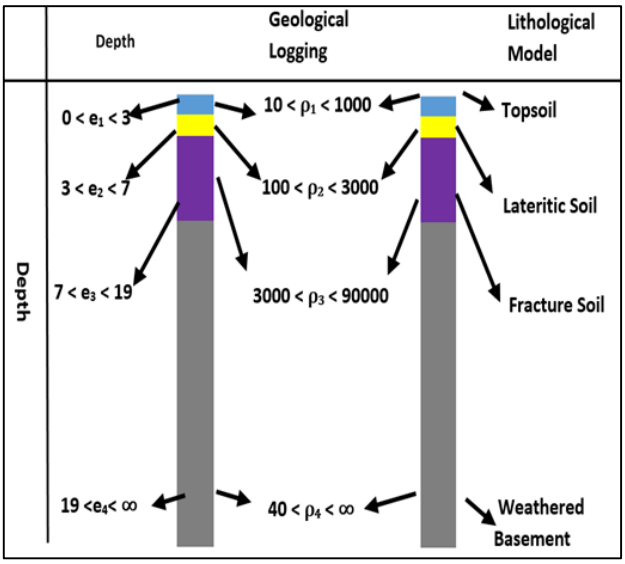

(a)

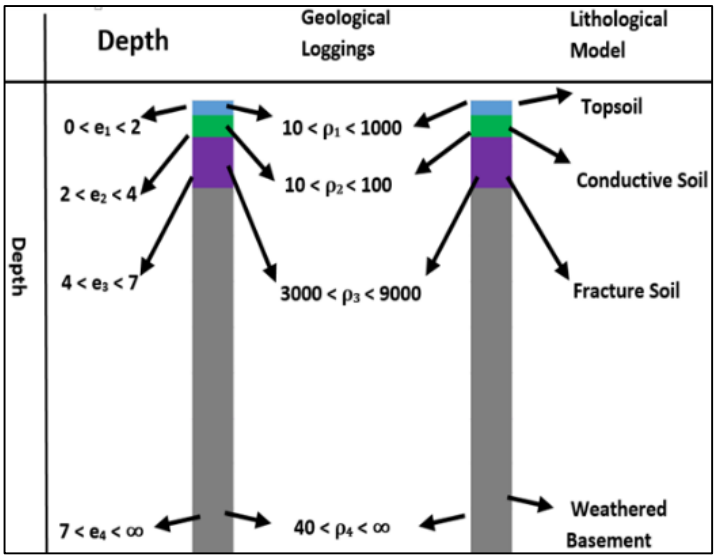

(b)

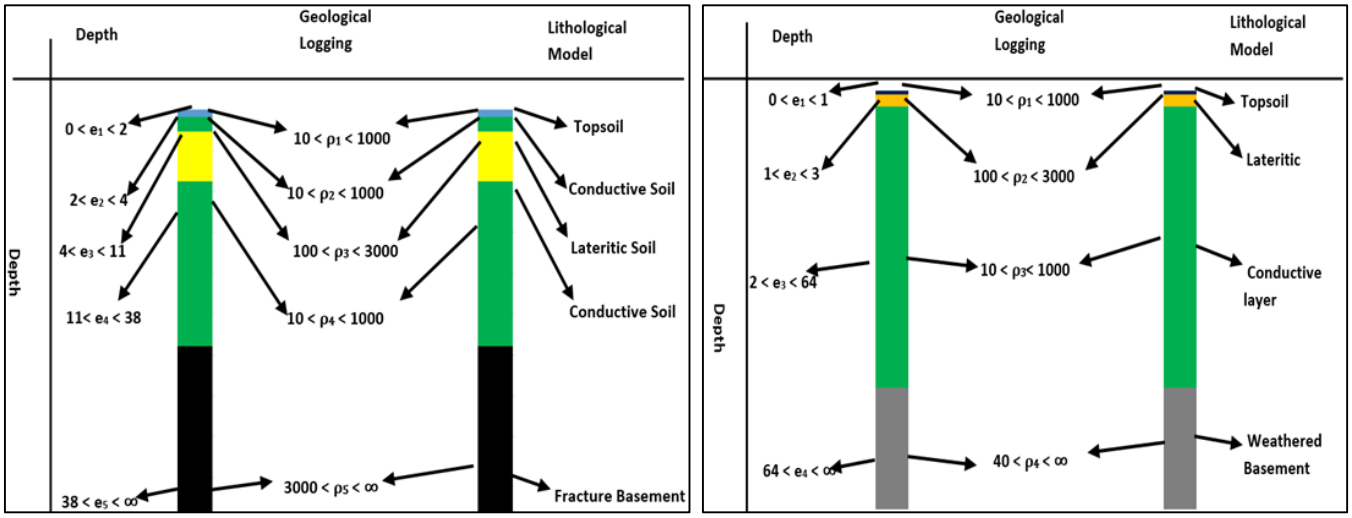

(c) (d)

Fig 12: Four representation of the nine Geo-electric section for Awka site 2

Table 1: Summary of VES result for Awka site 1

VES	Lat	Long	ρ(Ω)	∑ρ <5m	Depth	Thickness	Curves
1	691349	786263	5229	78549	1.28	1.28	
			1414		2.72	1.43	HKQ
			71906		4.62	2.9	
			6510		83.5	77.9	
			531				
2	691379	786373	60.8	16122.7	0.5	0.5	HKH
			12.2		0.92	0.42	
			16015		1.23	0.314	
			34.7		3.28	2.04	
			18.21				
3	691411	786494	2517	23132	0.5	0.5	KHK
			19064		0.911	0.411	
			1551		2.11	1.26	
			25146		7.76	5.6	
			262				
4	691366	786242	130	24460.9	0.5	0.5	HK
			22.9		0.387	0.887	
			24308		0.578	1.47	
			2528				
5	691403	786364	16248	97221	0.5	0.5	KHK
			80973		1.39	0.885	
			27151		10.71	9.29	
			5117		82.1	71.5	
			1284				
6	691440	786479	2515	11254	0.839	0.839	AKQ
			8739		4.32	3.48	
			37448		8.85	4.53	
			7462		84	75.2	
			179				
7	691397	786242	3.04	16.369	2.02	2.02	KHA
			12.7		1.86	3.88	
			0.629		3.45	7.33	
			1.75		69.2	76.6	
			164				
8	691429	786363	56.2	66.8	1.59	1.59	HKH
			10.6		3.52	1.94	
			212		11.6	8.04	
			18.3		38.2	26.4	
			4407				
9	691458	786406	24.5	30.59	1.05	1.05	HA
			6.09		3.09	2.04	
			650		69.3	66.3	
			1605				

Table 2: Summary of VES result for Awka site 2

VES	Lat	Long	ρ(Ω)	∑ρ at <5m	Depth	Thickness	Curves
10	695171	787995	1078	3432	0.5	0.5	AK
			2354		3.58	3.08	
			54228		5.65	2.07	
			1891				
11	695413	788039	117	117	2.99	2.99	AK
			763		6.18	3.19	
			95054		18.8	12.7	
			1479				
12	695683	788123	47.5	29898.5	1.58	1.58	AK
			146		1.83	3.41	
			29705		2.76	6.61	
			70.5				
13	695177	788154	49.6	49.6	0.649	0.649	H
			33		7.69	7.14	
			96.1				
14	695376	788187	347	356.47	1.37	1.37	HK
			9.47		1.68	0.306	
			31594		6.75	5.07	
			96.8				
15	695707	788241	250	316.8	0.709	0.709	K
			66.8		2.24	2.24	
			45.36				
16	695231	788325	4020	5014	0.665	0.665	HK
			994		1.61	0.943	
			59961		9.18	7.5	
			1931				
17	695467	788363	2355	2355	0.692	0.692	HA
			14219		17.5	16.8	
			1522		34.8	17.3	
			31814				
18	695774	788400	1241	1241	1.16	1.16	KA
			9312		16.7	17.9	
			782		14.7	32.6	
			266305				

Discussion

Geophysical resistivity methods are grounded on examining how the earth reacts to the movement of electrical current. The amount of water present primarily regulates the degree of conductivity variability when it comes to the shallow subsurface. By measuring the resistivity, we can ascertain the extent of water saturation and pore space connectivity. A growing amount of water content and higher salinity of subterranean water typically results in a reduction in the measured resistivity. Consequently, an increase in rock porosity and fracture count tends to decrease the measured resistivity if the voids contain water.

Soil pipes are mainly void spaces beneath the earth's surface or areas that have been greatly drained by run-off water in the subsurface. Soils that have been drained are known to have high resistivity (Beg *et al*., 2013 and Santos *et al*., 2006). The presence of soil pipes in the subsurface decreases the conductivity below ground values. In the dipole-dipole and VES surveys, areas with very high resistivity located near the surface of the profile were interpreted as potential soil pipe formation areas, while areas with moderate to high conductivity were interpreted as crystalline rocks. Crystalline rocks lack pore spaces (Onwuegbuchulam *et al*., 2013) [30].

The dipole-dipole surveys show six profiles' results from the 2D resistivity imaging obtained through an inversion method that was produced from nine iterations with a RMS error 7.4%. Due to the anisotropic characteristic of the study areas, the subsurface was divided into 6 distinct structures: saturated fault/fracture zones (10 -3000Ωm), clay (10 – 100Ωm), sandy clay (100 - 3000Ωm), sand (1000 - 10000Ωm), eroded soil (3000 - 30000Ωm) and bedrocks (3000Ωm to ∞). The high resistivity structures (≥ 3000Ωm), particularly those close to the surface of the profiles are interpreted as eroded structures, which encourages soil-piping formation because of their dispersive nature that is caused by differentiation of soil due run off rainwater (Joshi *et al*., 2021; Onda, 1994) [22, 29].

The VES surveys were specifically done on the profiles where the dipole-dipole surveys were carried out to determine the lithological models of the study areas and to delineate the piping paths. Eighteen soundings were performed and 11 different sounding curves were determined (H, K, KA, HA, HK, AK, HKQ, HKH, KHK, AKQ, and KHA) until a depth of 85m and 34m for Awka site I and Awka site II respectively. These sounding curves are characterized by conductive and fractured/weathered levels in the subsurface and are interpreted as electrical discontinuities resulting from the porosity of rocks or/and migration of fluid in the subsurface.

The geo-electric models obtained from the electrical characteristic (resistivity ρ, thickness t, and depth e) of the subsurface delineated three to five lithological models, which may include topsoil, conductive soil, lateritic soil, weathered/unsaturated fracture soil and basements with varying resistivity, thickness and depth for different sounding. Models with very high resistivity especially those

of the weathered/ unsaturated fracture soil that are close to surface of the profiles are interpreted as areas that could house the formation of soil pipes. The 2D and 3D maps (figure 11 and 12) of the surface gotten from resistivity that are $\leq 5m$ from the surface of the profiles, show the paths follow by soil pipes and they are found to follow the pattern of the stress direction (Ogbe and Osokor, 2020 and Amugo *et al*., 2010) and sloppy terrain of the surface area. (Bernatek-Jakiel & Poesen, 2018; Gilman & Newson, 1980; Joshi *et al*., 2021, 2021; Pierson, 1983) [3, 22, 33].

Conclusion

Two direct current surveys were conducted to investigate the special distribution, pattern and characteristic of soil piping that has developed in the subsurface of two-soil subsidence located at Awka, Anambra state, Nigeria.

The dipole- dipole survey delineated six different structures due to the structural anisotropic behavior of the study area. The eroded structure with resistivity 1200 - 30000Ωm and with strong dispersive soils were considered as structured that favours the formation of piping.

The result from the VES obtained along the dipole-dipole profiles were presented as overview of sounding, curves, geo-electric section and iso-resistivity map. The sounding curves show the variation of resistivity with depth. Depending on the electrical characteristic of the subsurface, 14 curves were depicted (H, K, KA, HA, HK, AK, HKQ, HKH, KHK, AKQ, and KHA). These abnormal distributions of resistivity with depth (35m and 85m) in addition to vertical changes in the subsurface gave rise to seven geo-electrical sections. The fracture/weathered layers and conductive layers divide the subsurface into areas that favours soil piping and one that prevent soil piping respectively. The 3D iso-resistivity mapping describes the pattern and paths of the soil piping in the subsurface and they follow the structural stressed pattern area, the fluid migration pattern in the subsurface and the sloppy terrain.

The D.C technique has proved to be an effective method for detecting and studying complex behavior of soil piping in the subsurface.

Acknowledgement

We will like to acknowledge the staff of Anambra state Ministry of Works and Anambra Material Laboratory.

Author Contributions

The two authors contributed equally to the success of this work.

Reference

1. Atallah N, Shakoor A, Watts CF. Investigating the potential and mechanism of soil piping causing water-level drops in Mountain Lake, Giles County, Virginia. Engineering Geology. 2015; 195:282-291. https://doi.org/10.1016/j.enggeo.2015.06.001.
2. Bernatek-Jakiel A, Kondracka M. Combining geomorphological mapping and near surface geophysics (GPR and ERT) to study piping systems. Geomorphology. 2016; 274:193-209. https://doi.org/10.1016/j.geomorph.2016.09.018.
3. Bernatek-Jakiel A, Poesen J. Subsurface erosion by soil piping: Significance and research needs. Earth-Science Reviews. 2018; 185:1107-1128. https://doi.org/10.1016/j.earscirev.2018.08.006
4. Bernatek-Jakiel A, Wrońska-Wałach D. Impact of piping on gully development in mid-altitude mountains under a temperate climate: A dendrogeomorphological approach. CATENA. 2018; 165:320-332. https://doi.org/10.1016/j.catena.2018.02.012
5. Bhagyalekshmi S, Mohan M, Sreedharan K, Ajaykumar B. Evaluation of the factors controlling the spatial distribution of soil piping: A case study from the southern Western Ghats, India. Arabian Journal of Geosciences. 2015; 8(10):8055-8067. https://doi.org/10.1007/s12517-015-1793-8
6. Blanco-Canqui H, Lal R. Principles of Soil Conservation and Management. Springer Netherlands, 2010. https://doi.org/10.1007/978-1-4020-8709-7
7. Borah UK, Gond A, Rajan PP, Sivan R, Vivekanandan N. Joint geomorphological and geophysical (electrical resistivity) investigation for the configuration of soil pipe. Contributions to Geophysics and Geodesy, 2022, 52(2). https://doi.org/10.31577/congeo.2022.52.2.4
8. Bryan RB. Soil erodibility and processes of water erosion on hillslope. Geomorphology. 2000; 32(3-4):385-415. https://doi.org/10.1016/S0169-555X(99)00105-1
9. Cardarelli E, Cercato M, De Donno G, Di Filippo G. Detection and imaging of piping sinkholes by integrated geophysical methods. Near Surface Geophysics. 2014; 12(3):439-450. https://doi.org/10.3997/1873-0604.2013051
10. Carrazza L, Moreira C, Portes L. Gully cavity identification through electrical resistivity tomography. Revista Brasileira de Geofísica, 2016, 34. https://doi.org/10.22564/rbgf.v34i2.799
11. Castañeda C, Javier Gracia F, Rodríguez-Ochoa R, Zarroca M, Roqué C, Linares R, *et al*. Origin and evolution of Sariñena Lake (central Ebro Basin): A piping-based model. Geomorphology. 2017; 290:164-183. https://doi.org/10.1016/j.geomorph.2017.04.013
12. Chibuogwu IU, Ugwu GZ. An Open Investigation of Some Soil Pipes Forming Soil Subsidence at Awka South Local Government Area Using Very Low Frequency Electromagnetic Geophysical Technique. International Journal of Scientific Research in Multidisciplinary Studies. 2023; 9(2):40-45.
13. García-Ruiz José M, Lasanta T, Alberto F. Soil erosion by piping in irrigated fields. Geomorphology. 1997; 20(3-4):269-278. https://doi.org/10.1016/S0169-555X(97)00028-7
14. Gibson PJ, Lyle P, George DM. Application of Resistivity and Magnetometry 1 Geophysical Techniques for Near-Surface Investigations in Karstic Terrains in Ireland. Journal of Cave 2 and Karst Studies. 2004; 66:35-38.
15. Gilman K, Newson MD. Soil Pipes and Pipeflow A Hydrological Study in Upland Wales. Geo Abstract, 1980, 100.
16. Got JB, Bielders CL, Lambot S. Characterizing soil piping networks in loess-derived soils using ground-penetrating Radar. Vadose Zone Journal, 2020, 19(1). https://doi.org/10.1002/vzj2.20006
17. Graham CB, Lin H. Chapter 18 - Subsurface Flow Networks at the Hillslope Scale: Detection and Modeling. In H. Lin (Ed.), Hydropedology, 2012, 559-593. Academic Press. https://doi.org/10.1016/B978-0-12-386941-8.00018-6

18. Holden J. Hydrological connectivity of soil pipes determined by ground-penetrating radar tracer detection. Earth Surface Processes and Landforms. 2004; 29(4):437-442. https://doi.org/10.1002/esp.1039
19. Holden J, Burt TP. Piping and pipeflow in a deep peat catchment. CATENA. 2002; 48(3):163-199. https://doi.org/10.1016/S0341-8162(01)00189-8
20. JO Coker, HH Akpan, AO Atilade, OF Ojo. Seasonal Comparison of Potential Groundwater Aquifer in Ijebu-Ife, South-West, Nigeria, using Dipole-Dipole Array and Electromagnetic Methods. Journal of the Nigerian Society of Physical Sciences, 2020, 241-249. https://doi.org/10.46481/jnsps.2020.128
21. Jones JAA, Richardson JM, Jacob HJ. Factors controlling the distribution of piping in Britain: A reconnaissance. Geomorphology. 1997; 20(3-4):289-306. https://doi.org/10.1016/S0169-555X(97)00030-5
22. Joshi M, Prasobh PR, Rajappan S, Rao BP, Gond A, Misra A, *et al*. Detection of soil pipes through remote sensing and electrical resistivity method: Insight from southern Western Ghats, India. Quaternary International. 2021; 575-576:51-61. https://doi.org/10.1016/j.quaint.2020.08.021
23. Leslie IN, Heinse R. Characterizing Soil-Pipe Networks with Pseudo-Three-Dimensional Resistivity Tomography on Forested Hillslopes with Restrictive Horizons. Vadose Zone Journal. 2013; 12(4):vzj2012.0200. https://doi.org/10.2136/vzj2012.0200
24. Li S, Liu B, Nie L, Liu Z, Tian M, Wang S, Su M, *et al*. Detecting and monitoring of water inrush in tunnels and coal mines using direct current resistivity method: A review. Journal of Rock Mechanics and Geotechnical Engineering. 2015; 7(4):469-478. https://doi.org/10.1016/j.jrmge.2015.06.004
25. Li ZX, Rao SW. The determination of frequency domain soil parameters of horizontally layered structure by using dipole-dipole array. International Journal of Numerical Modelling: Electronic Networks, Devices and Fields. 2019; 32(5):e2578. https://doi.org/10.1002/jnm.2578
26. Loke MH, Barker RD. Rapid least-squares inversion of apparent resistivity pseudosections by a quasi-Newton method1. Geophysical Prospecting. 1996; 44(1):131-152. https://doi.org/10.1111/j.1365-2478.1996.tb00142.x
27. Mi KP, Samgyu P, Myeong-Jong Y, Changryol K, Jung-Sul S, Jung-Ho K, *et al*. Application of electrical resistivity tomography (ERT) technique to detect underground cavities in a karst area of South Korea. Environ Earth Sci. 2013; 50(2):256-267.
28. Neyamadpour A, Wan Abdullah WAT, Taib S, Neyamadpour B. Comparison of Wenner and dipole-dipole arrays in the study of an underground three-dimensional cavity. Journal of Geophysics and Engineering. 2010; 7(1):30-40. https://doi.org/10.1088/1742-2132/7/1/003
29. Onda Y. Seepage erosion and its implication to the formation of amphitheatre valley heads: A case study at Obara, Japan. Earth Surface Processes and Landforms. 1994; 19(7):627-640. https://doi.org/10.1002/esp.3290190704
30. Onwuegbuchulam DO, Ikoro DO, Nwugha VN, Okereke CN. Application of Very Low Frequency-Electromagnetic (VLF-EM) Method to Map Fractures/Conductive Zones in Auchi South western Nigeria. The International Journal Of Engineering And Science (IJES). 2013; 5(5):07-13.
31. Parker GG, Higgins CG, Parker GG, Wood WW. Chapter 4. Piping and pseudokarst in drylands. In Geological Society of America Special Papers. 1990; 252:77-110. Geological Society of America. https://doi.org/10.1130/SPE252-p77
32. Patti G, Grassi S, Morreale G, Corrao M, Imposa S. Geophysical surveys integrated with rainfall data analysis for the study of soil piping phenomena occurred in a densely urbanized area in eastern Sicily. Natural Hazards. 2021; 108(3):2467-2492. https://doi.org/10.1007/s11069-021-04784-9
33. Pierson TC. Soil pipes and slope stability. Quarterly Journal of Engineering Geology. 1983; 16(1):1-11. https://doi.org/10.1144/GSL.QJEG.1983.016.01.01
34. Sidle RC, Kitahara H, Terajima T, Nakai Y. Experimental studies on the effects of pipeflow on through flow partitioning. Journal of Hydrology. 1995; 165(1):207-219. https://doi.org/10.1016/0022-1694(94)02563-Q
35. Ungureanu C, Adrian P, Adrian LB, Anton C. Use of electric resistivity tomography (ERT) for detecting underground voids on highly anthropized urban construction sites. Procedia Engineering. 2017; 209:13-16.
36. Vannoppen W, Verachtert E, Poesen J. Pipeflow response in loess-derived soils to precipitation and groundwater table fluctuations in a temperate humid climate: Pipeflow response to precipitation and groundwater table fluctuations. Hydrological Processes. 2017; 31(3):586-596. https://doi.org/10.1002/hyp.11049
37. Verachtert E, Maetens W, Van Den Eeckhaut M, Poesen J, Deckers J. Soil loss rates due to piping erosion: Soil Loss Rates Due To Piping Erosion. Earth Surface Processes and Landforms. 2011; 36(13):1715-1725. https://doi.org/10.1002/esp.2186.
38. Wilson GV, Wells R, Kuhnle R, Fox G, Nieber J. Sediment detachment and transport processes associated with internal erosion of soil pipes: Sediment detachment and transport in soil pipes. Earth Surface Processes and Landforms. 2018; 43(1):45-63. https://doi.org/10.1002/esp.4147
39. Zhang T, Wilson GV. Spatial distribution of pipe collapses in Goodwin Creek Watershed, Mississippi: Spatial Distribution of Pipe Collapses. Hydrological Processes. 2013; 27(14):2032-2040. https://doi.org/10.1002/hyp.9357
40. Zhu TX, Luk SH, Cai QG. Tunnel erosion and sediment production in the hilly loess region, North China. Journal of Hydrology. 2002; 257(1):78-90. https://doi.org/10.1016/S0022-1694(01)00544-3
41. Zohdy AAR. The Auxilliary Point Method of Electrical sounding Interpretation and its Relationship to Dar Zorrouk Parameters. Geophysics. 1965; 30:644-650.
42. Zohdy AAR, Eaton GP, Mabey DR. Application of Surface Geophysics to Groundwater Investigations. Techniques of Water Resources Investigations of U.S. Geol. Survey: Book 2, Chapter DI. U.S. Government Printing Office: Washington, D.C., USA, 1974, 66.
43. Koefoed O. Geosounding Principles, 1. Resistivity Sounding Measurements. Elsevier Scientific Publishing: Amsterdam, Netherlands, 1979, 275.
44. Keller GV, Frishchncht FC. Electrical Methods in

Geophysical Prospecting. Pergamon Press: New York, NY, 1966, 96.
45. Vander Velpen BPA. Win RESIST Version 1.0. Resistivity Sounding Interpretation Software. M.Sc. Research Project, ITC, Delft Netherland, 2004.
46. Environment and Social Management Plan. Introduction to Environment Basic Concept.Teaching conducting agency, 2016, 21-26.